# Cellulose Nanocrystal/Poly(ethylene glycol) Composite as an Iridescent Coating on Polymer Substrates: Structure-Color and Interface Adhesion

Mingyue Gu,[†] Chenyu Jiang,[†] Dagang Liu,*,[†,‡] Nana Prempeh,[†] and Ivan I. Smalyukh[‡]

[†]Collaborative Innovation Center of Atmospheric Environment and Equipment Technology, Nanjing University of Information Science and Technology, Nanjing 210044, P. R. China

[‡]Department of Physics, University of Colorado, Boulder, Colorado 80309, United States
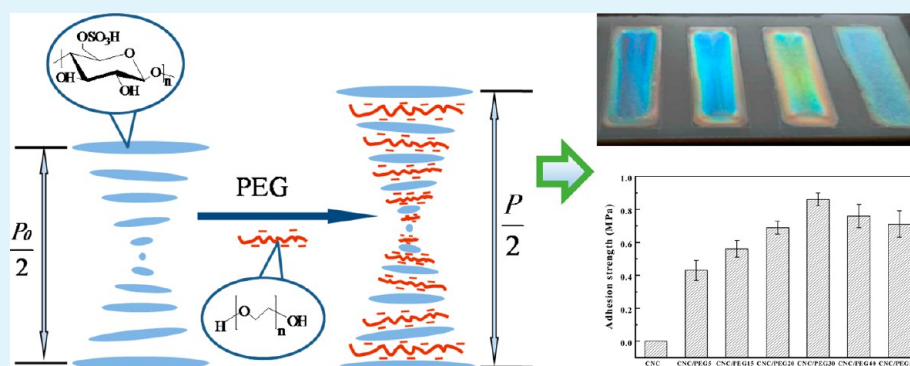
ABSTRACT: The broad utility as an environmentally friendly and colorful coating of cellulose nanocrystal (CNC) was limited by its instability of coloration, brittleness, and lack of adhesion to a hydrophobic surface. In the present work, a neutral polymer, poly(ethylene glycol) (PEG) was introduced into CNC coatings through evaporation-induced self-assembly (EISA) on polymer matrices. The structure-color and mechanical properties of the composite coating or coating film were characterized by UV−vis spectroscopy, polarized light microscopy (PLM), scanning electron microscopy (SEM), wide-angle X-ray diffraction (WXRD), and tensile tests. Results showed that the reflective wavelength of the iridescent CNCs could be finely tuned by incorporation of PEG with varied loadings from 2.5 to 50 wt %, although the high loading content of PEG would produce some side effects because of the severe microphase separation. Second, PEG played an effective plasticizer to improve the ductility or flexibility of the CNC coating or coating film. Furthermore, as a compatibilizer, PEG could effectively and tremendously enhance the adhesion strength between CNCs and neutral polymer matrices without destroying the chiral nematic mesophases of CNCs. Environmentally friendly CNC/PEG composites with tunable iridescence, good flexibility, and high bonding strength to hydrophobic polymer matrices are expected to be promising candidates in the modern green paint industry.

KEYWORDS: cellulose nanocrystal, poly(ethylene glycol), polymer substrate, iridescent coatings, cholesteric liquid crystal, interface adhesion

INTRODUCTION

Volatile organic compounds (VOCs) mainly emanating from solvents in industrial painting or adhesives[1−3] pose major health concerns because of their high toxicity and consistent concentrations in ambient air.[4] In the atmosphere, these compounds aid in the formation of secondary organic aerosols and ozone in the troposphere. For decades, regulatory agencies in most industrialized nations have enacted more and more stringent measures and regulations on the applications of VOCs to help control the solvent content in coatings. These VOC regulations have also spurred the growth of low-VOC technologies, such as water-borne,[5,6] powder,[7,8] high solids,[9] and energy-curable coatings.[10]

Several methods have already been used to generate colorful coatings via chemical reaction between inorganic salts and sodium stearate or grafting with polyfluorinatedazo dyes,[11,12] however, these processes are associated with many serious pollution problems and high production cost. Recently, chiral nematic or cholesteric liquid crystal (CLC) with self-organized helical superstructures have shown great potential in colorful coating applications due to their specific optical properties, that is, CLC can present a beautiful, never-faded, reflective visible coloration under incident light generating from its unique helical nematic structure. However, most of these cholesteric liquid crystals are normally synthesized from aromatic polyester or polyamide resins, which has led to adverse pollution issues coupled with high cost of production.[13,14]

As a new cholesteric liquid crystal, cellulose nanocrystals (CNCs) prepared by acid hydrolysis of cellulose have shown anisotropic spindle-like shapes and high surface charge imparted by the use of strong acids such as H_2SO_4 during hydrolysis, and thus can generate mesophases of chiral nematic liquid crystal at low concentrations.[15−17] Interestingly, the chiral nematic ordering can be preserved in a solidified film through evaporation-induced self-assembly (EISA) of CNC colloidal dispersion, thereby leading to structural color exhibited in solid films.[17] The unique optical properties of solidified films with chiral nematic order have been exploited as liquid crystal templet, flexible and iridescent composite films,[18−20] optical sensors,[21] and filters.[22] CNCs are anticipated to be used as a colorful and environmental-friendly coating to substitute the conventional hazardous coating containing VOCs. However, as far as we know very few works on CNC coatings were reported. Tuning the coloration by modifying the structure of the chiral-nematic organization and improving the interface compatibility of CNCs with substrate is essential for developing optical coating materials. Various processes such as the addition of salts,[23−25] treatment by sonication, or homogenization[24] had been well-established and proven to be good tuning techniques which cause a red-shift in solid films,[26] however, the addition of monovalent salts, such as NaCl, would lead to a blue-shift.[23,25,27] As a matter of fact, regardless of the variation of shift in reflection wavelength, the chirality and the equilibrium between hydrogen bonding affinity and surface charge repulsion among CNCs have vital impacts on the structure-effects of chiral nematic mesophases in a suspension or solidified film.[28] It is worth mentioning that several limitations exist for monovalent salt modified CNCs or mechanically treated CNCs, namely:

(i) irreversible inhibiting effect on the self-organization of CNCs;

(ii) coloration tuning in a limited range of ionic strengths;

(iii) agglomeration of nanocrystals and colloidal gelation caused by adding excess salt (C_{max} > 20 mM); and

(iv) brittleness nature for inappropriate application as surface coatings.[29]

To address these issues, we attempted to employ neither electrolytes nor polyelectrolytes in this study, instead, polyethylene glycol (PEG), a neutral polymer with excellent compatibility and affinity with CNCs was used to modulate the coloration of the coatings and also improve the flexibility and adhesion to polymeric substrates.

■ EXPERIMENTAL SECTION

Materials. Microcrystalline cellulose (MCC, column chromatography) and sulfuric acid were purchased from Sinopharm Chemical Reagent Co., Ltd., Shanghai, China. Regenerated cellulose dialysis tubing having a molecular weight cutoff of 8000−10 000 was supplied by Nanjing Wanqing Chemical Glassware Instrument Co., China. PEG (M_w = 20 000) was purchased from Aldrich Co. and used without further purification.

Preparation of CNCs. CNCs were prepared according to the method of sulfuric acid hydrolysis of MCC as described in our previous work.[17] Briefly, 4.0 g MCC was hydrolyzed by using 80 mL 64 wt % sulfuric acid under constant stirring in a water bath at 50 °C for about 2 h. Immediately following the acid hydrolysis, the suspension was diluted at least 5-fold with deionized water to quench the reaction. The diluted suspension was poured into the dialysis tubing and dialyzed against deionized water for several days to remove excess acid, low molecular weight saccharides, and other water-soluble

impurities. The final pH was at around 6.0 and the solid content of the resultant aqueous suspension of CNCs was approximately 0.5 wt %.

Preparation of CNC/PEG Nanocomposite Coatings. A specific amount of PEG solution (5 wt %) was dropped into CNC suspensions (0.5 wt %), and then the mixed suspension was gently sonicated for 2 min at 200 W. The suspension was subsequently concentrated into 2 wt % dispersions by slow evaporation at ambient condition, and degassed for about 6 min to obtain the concentrated CNC/PEG coating dispersions. Four different smooth resins, including ABS (polyacrylonitrile-butadiene-styrene), PC (polycarbonate), POM (polyformaldehyde), and PA (polyamide) were used as comparable coating substrates. Subsequently, composite dispersions were loaded onto the substrates and allowed to slowly evaporation-induced self-assemble into coatings for 48 h at room temperature. The resultant coatings with content of PEG varied from 2.5, 5, 7.5, 10, 15, 20, 30, 40, to 50 wt %, were labeled as CNC/PEG2.5, CNC/PEG5, CNC/PEG7.5, CNC/PEG10, CNC/PEG15, CNC/PEG20, CNC/PEG30, CNC/PEG40, and CNC/PEG50, respectively. Furthermore, CNCs and CNC/PEG free-standing coating films were prepared by casting on PTFE (polytetrafluoroethylene) substrates and then carried out morphology, optical, and mechanical tests.

Characterization. Reflection spectra were recorded on a UV−vis Shimadzu 3600 spectrophotometer and measured at normal incidence and room temperature in the spectral range from 300 to 800 nm. The texture of the chiral nematic mesophases in the CNCs and CNC/PEG was observed by polarized light microscope (LV100POL, Nikon, Japan). The cross section of coating films and the fractured surface of coatings were sputter-coating with gold for 1 min and then loaded on an S-4700 scanning electron microscope (SEM, Hitachi, Japan) with an accelerating voltage of 15 kV for observation and photographs. Fourier transform infrared spectra (FTIR) were recorded on a Nicolet-5700 FTIR spectrometer (Thermo Electron, U.S.A.) using KBr disk method in the range 4000−400 cm^{-1}. Contact angle measurement using a sessile-drop technique was performed on a CAM200 goniometer (KSV, Finland) equipped with a CCD camera in a relative humidity of 10−25% at room temperature. Pure CNCs suspension or CNC/PEG composite suspension as a probe liquid were syringed dropwise on the surface of 5 different substrates under the control of a microsyringe pump (Hamilton-Bonaduz). Unless otherwise specified, each measurement was carried out at different spots and repeated more than 3 times.

The crystallinity and the phase structure of CNCs and CNC/PEG were conducted using a wide-angle X-ray diffractometer (XRD-6100, Bruker Siemens, Japan) with a Nickel-filtered Cu Kα radiation (λ = 1.524 Å) source at 40 kV and 30 mA. Diffraction data were collected from 2θ = 4 to 60° in steps of 2°/min at room temperature. The degree of crystallinity (DC) of the CNCs and CNC/PEG were evaluated using the following equation:

$$DC = \frac{S}{S_0} \times 100\%$$

(1)

where S is the sum of the areas of all the crystallinity peaks and S_0 is the total area under diffractogram.

Tensile testing was carried out on a universal testing machine equipped with a 500 N load cell at room temperature (SLBL-500, Shimadzu, Japan). The test specimen dimensions were 60 × 10 × ~0.15 mm^3 (length × width × thickness). At least 5 specimens were parallelly tested at a nominal strain rate of 1 mm/min. A Pull-off adhesion tester (PosiTest; Defelsko Corporation, U.S.A.) was used to measure the adhesion strength of the coatings on different substrates. An aluminum dolly with diameter of 20 mm was glued onto the coating surface with an epoxy resin. After drying for 24 h at room temperature, the test zone was isolated and the dolly was pulled away from the polymer substrate perpendicularly. The strength required to pull away the coatings from substrates was recorded, and the results were averaged over 5 trials on each substrate.

■ RESULTS AND DISCUSSION

Structure of CNC/PEG. FTIR spectra of CNCs, PEG, and CNC/PEG composites are shown in Figure 1. Pure CNCs
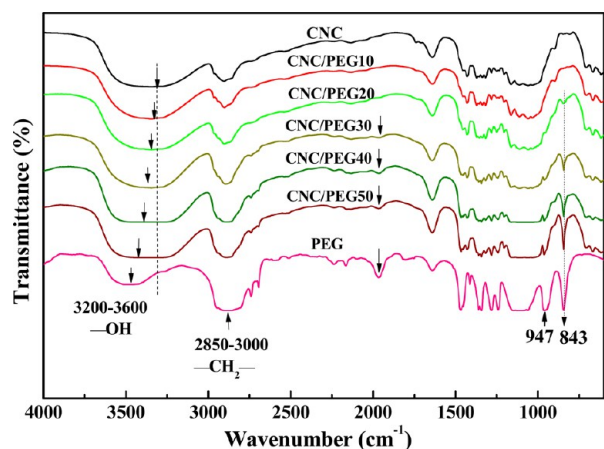

Figure 1. FTIR spectra of CNCs and CNC/PEG coating films.

exhibited absorption bands of 3200−3600, 2850−3000, and 1050−1150 cm^{-1} attributed to stretching modes of —OH, —CH$_2$—, and —O—, respectively.[30,31] Pure PEG exhibited distinct peaks at 1280, 947, and 843 cm^{-1}. By the addition of PEG, the composites exhibited strengthened absorption bands at 947 and 843 cm^{-1}, corresponding to the out-of-plane bending vibrations of C—H and O—H of the crystalline region in PEG.[32] Meanwhile, the maximum peak at around 3300 cm^{-1} of CNCs with the incorporation of PEG slightly shifted toward high frequency probably due to the hydrogen-bonding interactions between hydrophilic hydroxyl groups on the surface of the CNCs and the hydroxyl groups of the PEG chains.

XRD patterns of CNCs and CNC/PEG free-standing coating films are shown in Figure 2. Typical diffraction peaks at 14.8°,
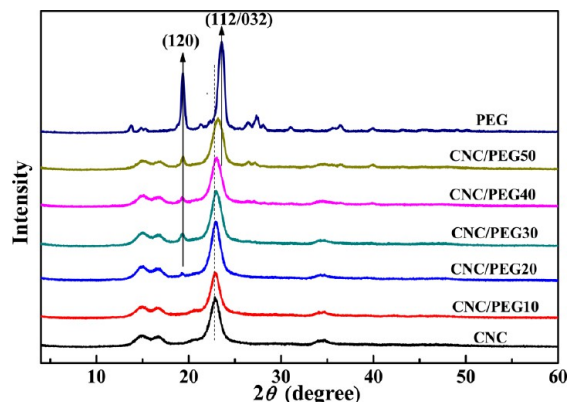

Figure 2. XRD patterns of PEG and CNCs, CNC/PEG10, CNC/PEG20, CNC/PEG30, CNC/PEG40, and CNC/PEG50 coating films.

16.3°, and 22.6°, corresponding to the (1$\bar{1}$0), (110), and (200) characteristic crystallographic planes of cellulose I crystal,[33] respectively, were exhibited in CNCs and CNC/PEG samples, suggesting that the crystal structure of CNCs was essentially preserved in CNC/PEG nanocomposites with the introduction of PEG. Meanwhile, it was interesting that several new diffraction peaks arose at 2θ = 19.2° and 23.2°, corresponding

to the (120) and (112)/(032) reflections from the PEG crystallites when the content of PEG was higher than 30 wt %.[34,35] Moreover, the intensity of the peaks at 2θ = 19.2° and 26.8° increased noticeably with the increasing content of PEG from 30 to 50 wt %. When the content of PEG in the composite was increased up to 50%, the diffraction peak at 22.6° of CNCs shifted toward the diffraction peak at 23.2° of PEG. The degree of crystallinity of CNCs, CNC/PEG10, CNC/PEG20, CNC/PEG30, CNC/PEG40, CNC/PEG50, and PEG were 79.49%, 82.68%, 83.89%, 84.06%, 76.02%, 74.99%, and 83.69%, respectively, indicating that crystallinity of the composites increased with an increment of PEG content (≤30 wt %). However, the crystallinity of the composites decreased when doped with an excess of PEG (>30 wt %) into the nanocrystals. That is to say, the alignment of LC mesophases was stable at a low loading of PEG with higher crystallinity, thus imparting positive effects on the crystallization of the composite; nonetheless, high loading PEG would result in an increment of crystalline domain of PEG and microphase separation, and furthermore disrupted the uniform alignment of mesophases of CNCs, thus leading to a slight decline of crystallinity of the bulk coating film samples of CNC/PEG40 and CNC/PEG50.[36]

Color-Tuning Effects of PEG. Figure 3 shows PLM micrographs of CNCs (a), CNC/PEG5 (b), CNC/PEG10 (c),
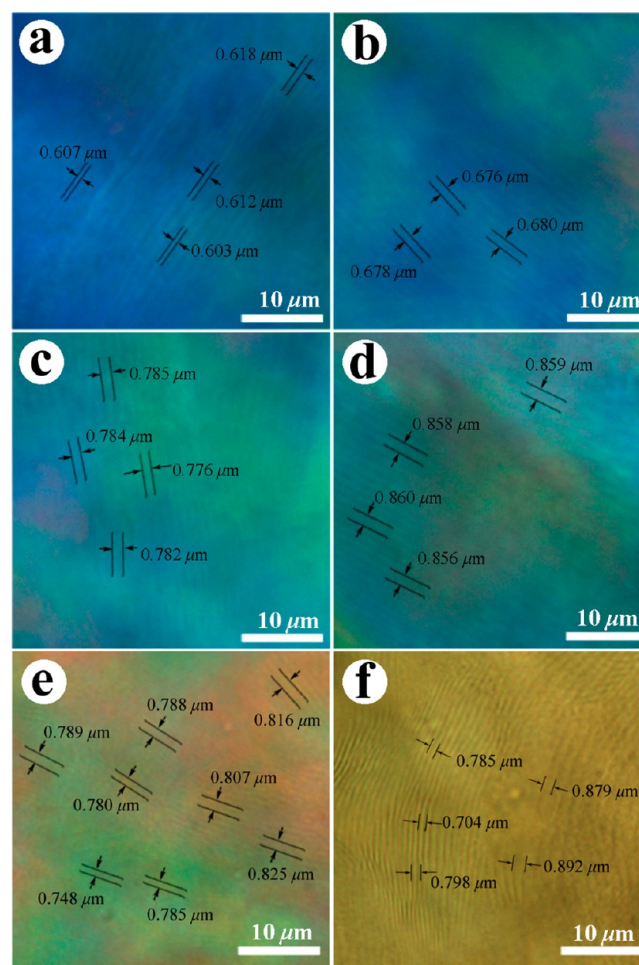

Figure 3. PLM micrographs of CNCs (a), CNC/PEG5 (b), CNC/PEG10 (c), CNC/PEG30 (d), CNC/PEG40 (e), and CNC/PEG50 (f) coating films.

CNC/PEG30 (d), CNC/PEG40 (e), and CNC/PEG50 (f), respectively. The chiral nematic phase in pure CNCs and CNC/PEG coating films was revealed by the presence of fingerprint texture.[37] The half cholesteric pitch, defined as the distance required for the CNCs rods to make a 180° rotation, namely the distance between two neighboring planar textures, dramatically increased from 0.612 (±0.008) μm to 0.680 (±0.004), 0.781 (±0.006), 0.858 (±0.003), 0.793 (±0.054), and 0.879 (±0.105) μm, with the increase of PEG from 0 to 5, 10, 30, 40, and 50 wt %, respectively. Correspondingly, the reflective color gradually shifted from bluish violet (Figure 3a) to bluish green (Figure 3b), yellowish green (Figure 3c), and yellowish brown (Figure 3d), specifying a red-shift in the visible reflective wavelength with the increase of PEG content. The PLM micrographs of CNC/PEG40 (Figure 3e) and CNC/PEG50 (Figure 3f) exhibited a multipitch texture and heterogeneous distribution of coloration since the long-range ordered mesophases became separated and disrupted by doping an excess of PEG into CNCs as indicated by XRD results.[28]

Figure 4 shows UV−vis spectra of CNCs and CNC/PEG free-standing coating films (a) and wavelength of maximum reflectivity (λ_{max}) measured as a function of PEG content (b). All coating films showed a high reflectivity (~70%) measured by UV−visible spectroscopy at a normal incidence. With

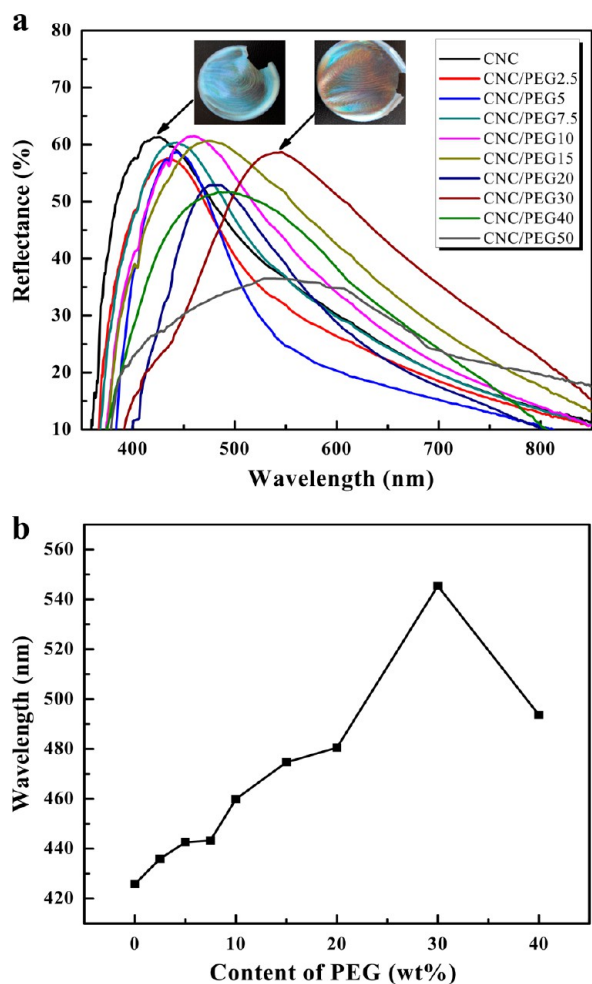increasing amounts of PEG from 0 to 2.5, 5, 7.5, 10, 15, 20, 30 wt %, the λ_{max} of coating films displayed a gradual redshift from 425 nm to 435, 442, 443, 460, 475, 481, and 545 nm, accordingly. As shown in the inset of Figure 4, CNCs and CNC/PEG30 films exhibited reflected bright iridescence in naked view under diffuse incident light, and displayed a blue, and orange coloration, respectively. That is to say, the λ_{max} of the iridescent CNCs film could be finely tuned from blue to red by dramatically adjusting the content of incorporated PEG. However, while the content of PEG exceeded 30 wt %, the coloration of the free-standing coating films did not appear as uniform as that of the films containing less PEG (≤30 wt %). Meanwhile, the λ_{max} of the CNC/PEG40 and CNC/PEG50 films were 494 and 516 nm, respectively, which was slightly reduced in comparison with that of CNC/PEG30. The reflection spectra of CNC/PEG50 exhibited a broad bandwidth and low reflectivity, which corresponds to polydomain mesophases of CNCs with widely distributed chiral pitches as observed from PLM (Figure 3f).

Suppose that the observed pitch was uniformly distributed in a birefringent film, the reflection of light unto the chiral nematic mesophases of CNCs and CNC/PEG would follow the Bragg reflection:

$$\lambda = n_{avg}\frac{P}{2}\sin\theta \qquad (2)$$

where n_{avg} is the average refractive index; $P/2$ is one-half of the helical pitch; and θ is the angle of incidence. Once n_{avg} and θ are constant, the relationship between λ and $P/2$ is linear. Theoretically, n_{avg} of the different composite films should be essentially constant with low content of PEG because the two components, PEG and CNCs, have similar refractive indices of 1.47 and 1.54, respectively. Hence, the increase in λ_{max} for samples with low PEG content could therefore be attributed to an increase in pitch.[28] Namely, due to the similar multihydroxyl pendant groups, PEG had good compatibility and affinity with CNCs and thereby PEG easily penetrated into nematic layers of mesogenic phases and acted as a homogeneously dispersant of CNCs. As a result, the spacing between neighboring nematic layers (P) was enlarged, and ultimately leading to the increase of reflective wavelength (red-shift). This is why a linear relationship between λ and P is revealed when the content of PEG is less than 30 wt % (Figure 4b). However, CNC nanocrystals interacted with each other and attempted to maintain a balance between the electronic repulsion generated from negative surface charges and hydrogen bonding attraction caused by multihydroxyls. The interaction is vital for the formation of long-range orientation and short-range positional order of helical chiral nematic hierarchy of CNCs.[28] Meanwhile, an excess amount of PEG chains penetrated into nematic layers and would weaken the repulsion and/or affinity interaction, thereby cutting-off or breaking the long-range orientation of mesophases of CNCs and forming independent crystalline phases of PEG. That is why nonlinear relationship between λ and P is revealed when the content of PEG is higher than 30 wt % (Figure 4b).

Morphological change as shown in Figure 5 provided further confirmation of the preservation and transition of chiral nematic organization in the CNC/PEG coating films. The thickness of coating films under SEM observation was around 96 μm. Pure CNCs and CNC/PEG coating films appeared very smooth on its top surface, but perpendicular to the top surface of nanocrystal layers with defects arose from changes in
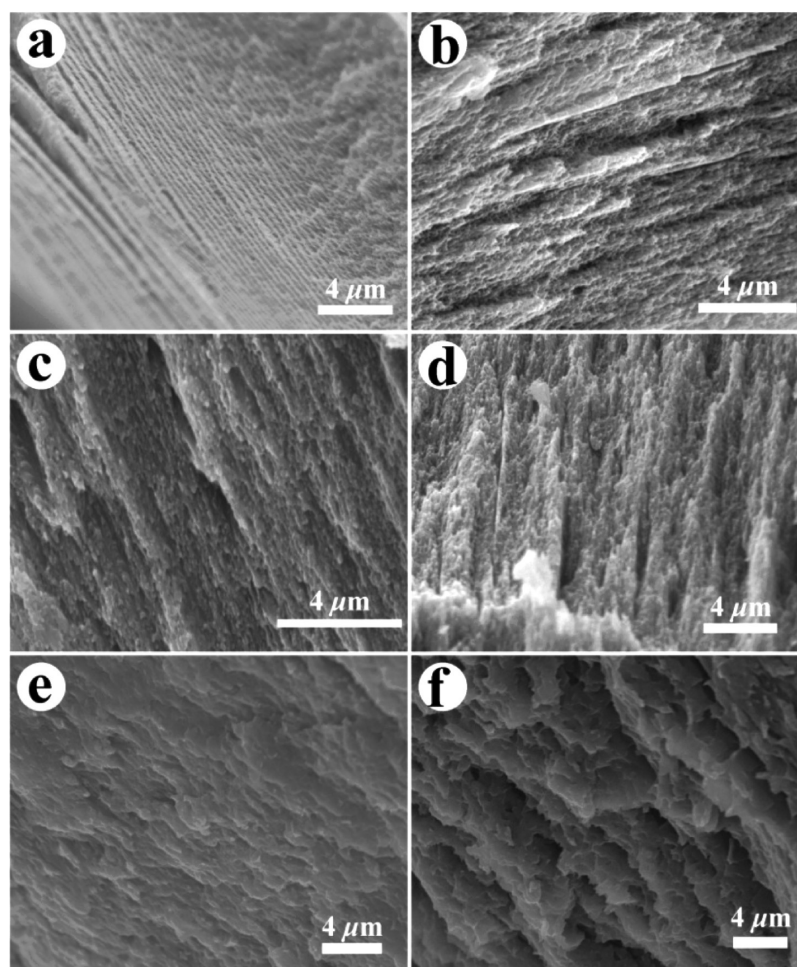
Figure 4. UV−vis spectra of CNCs and CNC/PEG coating films (a) and the λ_{max} measured by UV−vis spectroscopy as a function of PEG content (b).

Figure 5. SEM micrographs of the cross sections of CNCs (a), CNC/PEG10 (b), CNC/PEG20 (c), CNC/PEG30 (d), CNC/PEG40 (e), and CNC/PEG50 (f) coating films.

direction of the helical axis of the chiral nematic phase. Under high magnification, the repeating distance ($P/2$) was of the order of several hundred nanometers, and enlarged with the increment of PEG. Once the content of PEG was beyond 30 wt %, the repeating layers became ambiguous, indicating the partial loss of long-range orientation of nematic mesophases. Hence, the results from SEM are in agreement with the above-discussed mechanism as identified by PLM and reflective spectra.

Effects of PEG on the mechanical properties of CNC/PEG. Tensile strength, tensile modulus and elongation at break of CNC/PEG coating films are shown in Figure 6. It is worth to mention that the mechanical properties of pure CNC film could not be obtained since the film was too brittle to be measured. The elongation at break of CNC/PEG10, CNC/PEG20, CNC/PEG30, CNC/PEG40, and CNC/PEG50 were 0.67%, 2.37%, 2.63%, 4.10%, and 4.58%, respectively, indicating a continuous increase of strain at fracture with the incorporation of flexible PEG. Specifically, the elongation at break of CNC/PEG40 was 6.1 times higher than that of CNC/PEG10, indicating a high improvement of flexibility. However, the tensile strength and Young's modulus of CNC/PEG coating films decreased upon the increase of the PEG content from 10 to 50 wt %. The reductions in tensile strength and Young's Modulus of the CNC/PEG40 were 45% and 7.5%, respectively, as compared with those of the CNC/PEG10. That
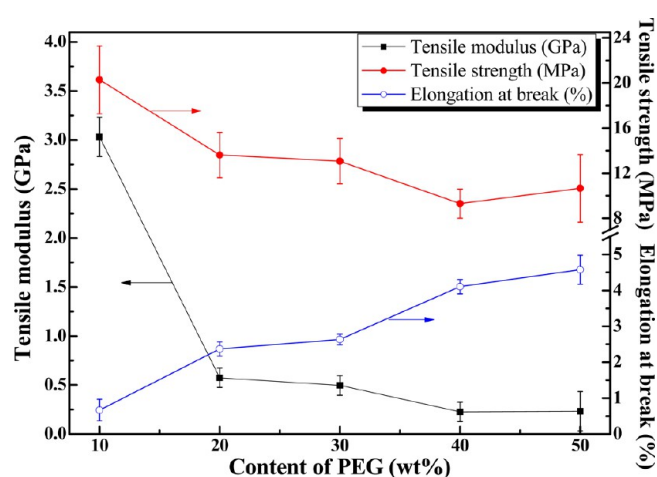

Figure 6. Tensile strength (●), tensile modulus (■), and elongation at break (○) of CNC/PEG coating films.

is to say, the ductility was improved with a slight loss of tensile strength. On the basis of the results of the tensile tests, PEG was definitely served as an effective plasticizer for CNCs. Meanwhile, the mechanical properties of CNC/PEG coating films could also be reflected by morphology of their cross sections observed by SEM as shown in Figure 5. CNCs (Figure 5a), CNC/PEG10 (Figure 5b), and CNC/PEG20 (Figure 5c)

demonstrated rather straight and smooth fractured cross sections with self-assembled structure of layer-by-layer. However, the fractured interface of CNC/PEG30, CNC/PEG40, and CNC/PEG50 (Figure 5d−f) became rough and undulating, indicating a highly improved ductility or flexibility in comparison with CNCs.

Interface Adhesion of CNC/PEG Coatings. Figure 7 shows the contact angle of coating dispersions of CNCs, CNC/
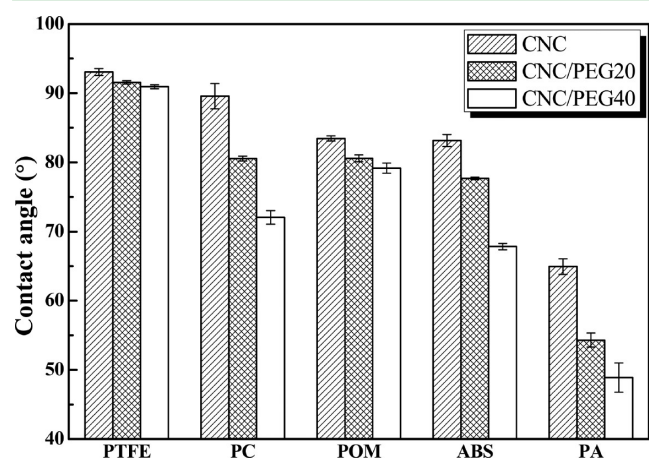

Figure 7. Contact angle for CNCs, CNC/PEG20, and CNC/PEG40 coating dispersions on substrates of PTFE, PC, POM, ABS, and PA, respectively.

PEG20, and CNC/PEG40 on 5 substrates of PTFE, PC, POM, PA, and ABS. Both CNCs and CNC/PEG have no attraction to PTFE substrate as evidenced by its high contact angle value (>90°), therefore, in this work, CNCs or CNC/PEG free-standing coating films could autopeel-off from PTFE matrices for the above-mentioned characterizations. However, CNC/PEG dispersions showed a good affinity to some other hydrophobic polymer matrices. For instance, with the

increasing PEG, CNC/PEG coating dispersions exhibited a decreasing trend in the contact angle value, owing to an improved affinity or compatibility between CNCs and hydrophobic substrates. Particularly on the PA substrate, the coating dispersions displayed the lowest contact angle among all substrates. That is to say, CNC/PEG showed a stronger affinity to PA than PTFE, PC, POM, or ABS, due to multihydrophilic amide, carboxyl, and amine groups of charged PA. Meanwhile, CNC dispersion on POM and ABS showed a similar contact angle, but CNC/PEG displayed a more significant drop for the contact angle value on ABS than that on POM with the increment of PEG. It is believed that amphiphilic PEG has hydrophobic main molecular chains and hydrophilic —OH groups which make it not only compatible with CNCs but also attractive to hydrophobic polymeric substrates. Interestingly, as shown in Figure 8A, no reflective iridescence could be visualized for dried CNCs and CNC/PEG coatings on PA substrates. When the coating was pulled off from the PA matrix, it was surprising that no fingerprint texture or birefringence could be visualized under PLM (Figure 8a) probably because the template induction effects of charged PA compelled CNCs to lose their original self-assembling drive generated from chirality and interaction among nanocrystals, thereby making it impossible to form layered chiral nematic mesophases in a very thin coating. As a result, neutral polymer (POM, ABS, and PC) other than charged polymer (PA) is selected as a preferred matrix for iridescent CNCs coating because the chiral nematic organization of CNCs could be preserved in the coatings. Moreover, the coloration of the coating could be tuned by incorporation of PEG. Photographs of CNC/PEG5, CNC/PEG15, CNC/PEG30, and CNC/PEG50 coatings on ABS substrates are shown in Figure 8B−B$_3$. The color of the CNC/PEG coating gradually turned from blue to red with the increase in PEG content, corroborating to the red-shift trend of the coating films cast on the PTFE. Unfortunately, in the case of the CNC/PEG50 coating, both the iridescence and the brightness faded away.
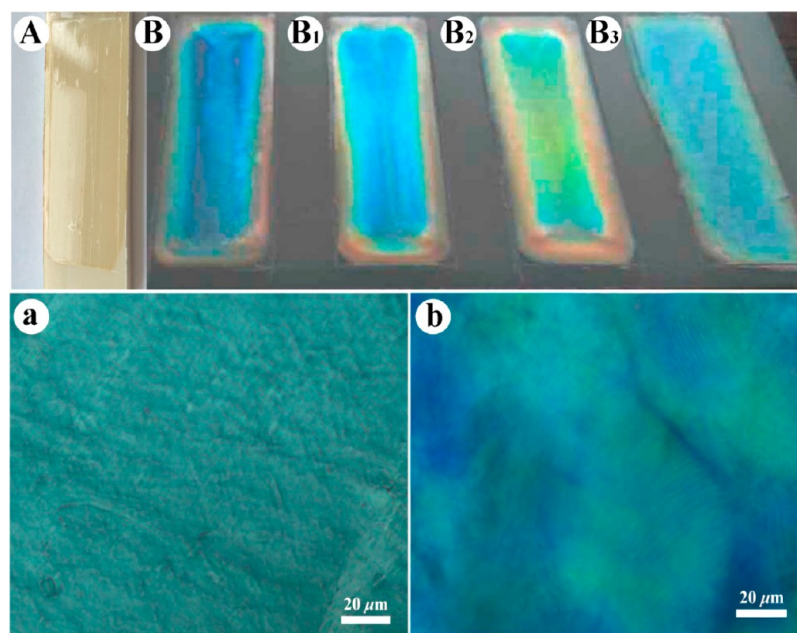

Figure 8. Photographs of CNC/PEG5 coating on PA (A), and CNC/PEG5 (B), CNC/PEG15 (B$_1$), CNC/PEG30 (B$_2$), and CNC/PEG50 (B$_3$) coatings on ABS; PLM micrographs of CNC/PEG5 coatings pulled off from PA (a) and ABS (b), respectively.

According to ASTM D4541 standard, the pull-off adhesion strengths between ABS substrates and CNC/PEG coatings are shown in Figure 9. The adhesion strength of CNC, CNC/
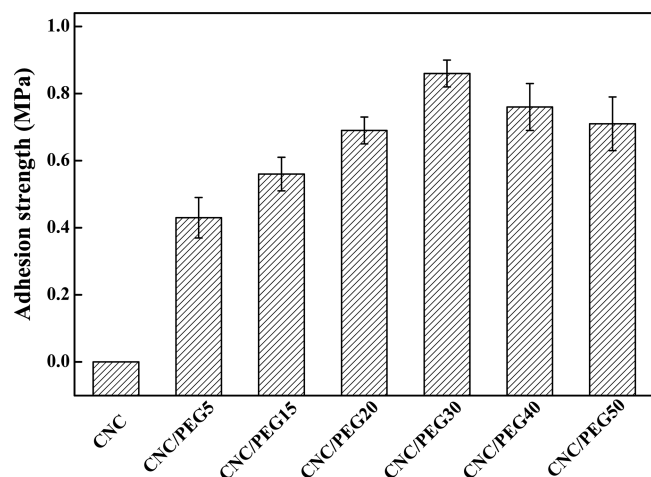

Figure 9. Pull-off Adhesion strength of CNCs, CNC/PEG5, CNC/PEG15, CNC/PEG20, CNC/PEG30, CNC/PEG40, and CNC/PEG50 coatings varnished on ABS substrates.

PEG5, CNC/PEG15, CNC/PEG20, CNC/PEG30, CNC/PEG40, and CNC/PEG50 coatings on ABS substrates were 0, 0.43, 0.56, 0.69, 0.86, 0.76, and 0.71 MPa, respectively. It is known that hydrophilic CNCs have no affinity to hydrophobic ABS, and that is why the pull-off strength of CNCs is zero. However, the adhesion strength of CNC/PEG on ABS substrate was effectively improved due to the incorporation of PEG, specifically, the adhesion strength of CNC/PEG30 coating was 2 times higher than that of CNC/PEG5 on ABS. Meanwhile, a slight decrease in the adhesion strength for both CNC/PEG40 and CNC/PEG50 was probably due to the phase separation between PEG crystalline phase and CNCs nematic

mesophases. The morphology of the fracture surface always provides some meaningful evidence to address the change of mechanical properties. Figure 10 shows micrographs of the fractural cross sections of CNCs, CNC/PEG15, CNC/PEG30, and CNC/PEG50 coatings resulting from the pull-off tests. CNCs peeled off from ABS and left nothing on the smooth substrate surfaces. The fracture surface of CNC/PEG coatings was rough (Figure 10b−d) as compared with that of pure CNCs (Figure 10a). With the increase of PEG, the interface adhesion between coating and substrates was strengthened and more coating residuals were detained on the interface (Figure 10b). Once the interface adhesion was stronger than the inner strength of the coating, the fracture occurred in the inner of coatings, e.g., the fracture surface of CNC/PEG30 and CNC/PEG50 coating showed a layered texture morph, indicating that the fracture took place in the inner of coating instead of the interface (Figure 10a,b). On the basis of the inner strength of all coating films as indicated in Figure 6, CNC/PEG30 shows the highest pull-off strength because it has a relative stronger interface adhesion than that of CNC/PEG with the content of PEG < 30 wt %, as well as a higher inner strength than that of CNC/PEG with the content of PEG > 30 wt %.

■ CONCLUSIONS

In this work, a neutral polymer, PEG, was employed to modulate the coloration as well as improve the flexibility of iridescent CNC coatings or coating films because PEG showed a good compatibility with CNCs due to the hydrogen-bonding interactions caused by their similar mesogenic moieties of multihydroxyl groups. Consequently, a great enhancement of coating adhesion and flexibility of coatings was achieved by incorporation of PEG, e.g., CNC/PEG10, CNC/PEG20, CNC/PEG30, CNC/PEG40, and CNC/PEG50 coating films cast on PTFE displayed an elongation at break of 0.67%, 2.37%, 2.63%, 4.10%, and 4.58%, respectively, suggesting an improved flexibility as compared with pure CNCs. The proper content of
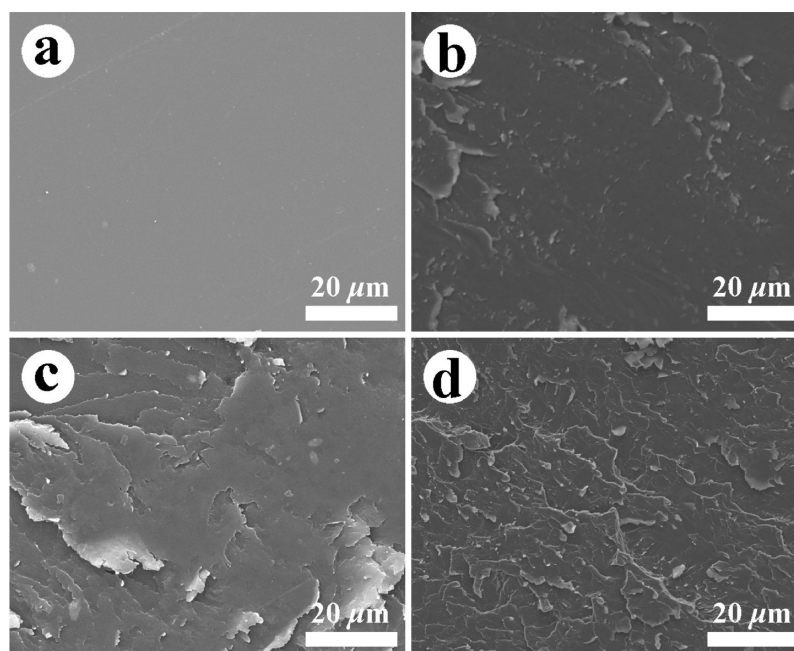

Figure 10. SEM micrographs of the fracture surfaces of CNCs (a), CNC/PEG15 (b), CNC/PEG30 (c), and CNC/PEG50 (d) coatings pulled off from ABS substrates, respectively.

PEG incorporated into CNCs also greatly improved the interface adhesion on the polymer matrix, e.g., the adhesion strength of the CNC/PEG30 coating on the ABS substrate was 2 times higher than that of CNC/PEG5. However, PEG acted as an efficient color tuner of CNC coatings while preserving the well-pronounced chiral nematic texture of pure CNCs, e.g. the addition of PEG at 30 wt % resulted in a red-shift of λ_{max} from 425 to 545 nm. As a consequence, CNC/PEG composite dispersions were successfully applied as iridescent coatings on neutral polymer matrices (POM, ABS, and PC) other than the charged PA matrix. However, an excess doping of PEG into CNCs would cause severe microphase separation between crystalline phases of PEG and chiral nematic mesophases of CNCs. On the basis of the testing results of mechanical properties and coloration distribution, CNC/PEG composites with loadings no more than 30 wt % PEG are excellent candidates of novel decorative, iridescence-controllable, glutinous, and environmentally-friendly coatings or paints.

■ AUTHOR INFORMATION

Corresponding Author

*Tel./Fax: +86-2558731090, E-mail: dagangliu@gmail.com; dagang@nuist.edu.cn (D.Liu).

ORCID Ⓓ

Dagang Liu: 0000-0002-1320-7030

Notes

The authors declare no competing financial interest.

■ REFERENCES

(1) Behera, S. N.; Betha, R.; Balasubramanian, R. Insights into Chemical Coupling among Acidic Gases, Ammonia and Secondary Inorganic Aerosols. *Aerosol Air Qual. Res.* **2013**, *13*, 1282−1296.

(2) Sumitsawan, S.; Cho, J.; Sattler, M. L.; Timmons, R. B. Plasma Surface Modified TiO$_2$ Nanoparticles: Improved Photocatalytic Oxidation of Gaseous *m*-Xylene. *Environ. Sci. Technol.* **2011**, *45*, 6970−6977.

(3) Dhada, I.; Nagar, P. K.; Sharma, M. Challenges of TiO$_2$-based Photooxidation of Volatile Organic Compounds: Designing, Coating, and Regenerating Catalyst. *Ind. Eng. Chem. Res.* **2015**, *54*, 5381−5387.

(4) Carratalá-Abril, J.; Lillo-Ródenas, M. A.; Linares-Solano, A.; Cazorla-Amorós, D. Activated Carbons for the Removal of Low-concentration Gaseous Toluene at the Semipilot Scale. *Ind. Eng. Chem. Res.* **2009**, *48*, 2066−2075.

(5) Wu, Z. F.; Wang, H.; Tian, X.; Cui, P.; Ding, X.; Ye, X. Z. The Effects of Polydimethylsiloxane on Transparent and Hydrophobic Waterborne Polyurethane Coating Containing Polydimethylsiloxane. *Phys. Chem. Chem. Phys.* **2014**, *16*, 6787−6794.

(6) Samyn, P.; Schoukens, G.; Stanssens, D.; Vonck, L.; Van den Abbeele, H. Hydrophobic Waterborne Coating for Cellulose Containing Hybrid Organic Nanoparticle Pigments with Vegetable Oils. *Cellulose* **2013**, *20*, 2625−2646.

(7) Vasilik, N. J.; Tyurin, Y. N.; Kolisnichenko, O. V.; Kovaleva, M. G.; Prozorova, M. S.; Arseenko, M. Y. Properties and Applications of Powder Coatings Formed by Multi-chamber Detonation Sprayer. *Appl. Mech. Mater.* **2013**, *467*, 179−184.

(8) Puig, M.; Cabedo, L.; Gracenea, J. J.; Jiménez-Morales, A.; Gámez-Pérez, J.; Suay, J. J. Adhesion Enhancement of Powder Coatings on Galvanised Steel by Addition of Organo-modified Silica Particles. *Prog. Org. Coat.* **2014**, *77*, 1309−1315.

(9) Hein, R. W. Driers for High-solids Coatings. *J. Coat. Technol.* **1999**, *71*, 21−25.

(10) Ryu, M. J.; Gang, S. N.; Lim, S. H. Effect of Silica Coating on Bond Strength Between a Gold Ally and Metal Bracket Bonded with Chemically Cured Resin. *Korean J. Orthod.* **2014**, *44*, 105−112.

(11) Soler, R.; Salabert, J.; Sebastián, R. M.; Vallribera, A.; Roma, N.; Ricart, S.; Molins, E. Highly Hydrophobic Polyfluorinated Azo Dyes Grafted on Surfaces. *Chem. Commun.* **2011**, *47*, 2889−2891.

(12) Ogihara, H.; Okagaki, J.; Saji, T. Facile Fabrication of Colored Superhydrophobic Coatings by Spraying a Pigment Nanoparticle Suspension. *Langmuir* **2011**, *27*, 9069−9072.

(13) Saha, A.; Tanaka, Y.; Han, Y.; Bastiaansen, C. M. W.; Broer, D. J.; Sijbesma, R. P. Irreversible Visual Sensing of Humidity Using a Cholesteric Liquid Crystal. *Chem. Commun.* **2012**, *48*, 4579−4581.

(14) White, T. J.; McConney, M. E.; Bunning, T. J. Dynamic Color in Stimuli-responsive Cholesteric Liquid Crystals. *J. Mater. Chem.* **2010**, *20*, 9832−9847.

(15) Habibi, Y.; Lucia, L. A.; Rojas, O. Cellulose Nanocrystals: Chemistry, Self-assembly, and Applications. *Chem. Rev.* **2010**, *110*, 3479−3500.

(16) Klemm, D.; Kramer, F.; Moritz, S.; Lindström, T.; Ankerfors, M.; Gray, D.; Dorris, A. Nanocelluloses: a New Family of Nature-based Materials. *Angew. Chem., Int. Ed.* **2011**, *50*, 5438−5466.

(17) Liu, D.; Chen, X.; Yue, Y.; Chen, M.; Wu, Q. Structure and Rheology of Nanocrystalline Cellulose. *Carbohydr. Polym.* **2011**, *84*, 316−322.

(18) Shopsowitz, K. E.; Qi, H.; Hamad, W. Y.; MacLachlan, M. J. Free Standing Mesoporous Silica Films with Tunable Chiral Nematic Structures. *Nature* **2010**, *468*, 422−425.

(19) Giese, M.; Khan, M. K.; Hamad, W. Y.; MacLachlan, M. J. Imprinting of Photonic Patterns with Thermosetting Amino-form-aldehyde-cellulose Composites. *ACS Macro Lett.* **2013**, *2*, 818−821.

(20) Bardet, R.; Belgacem, N.; Bras, J. Flexibility and Color Monitoring of Cellulose Nanocrystal Iridescent Solid Films Using Anionic or Neutral Polymers. *ACS Appl. Mater. Interfaces* **2015**, *7*, 4010−4018.

(21) Zhang, Y. P.; Chodavarapu, V. P.; Kirk, A. G.; Andrews, M. P. Structured Color Humidity Indicator from Reversible Pitch Tuning in Self-assembled Nanocrystalline Cellulose Films. *Sens. Actuators, B* **2013**, *176*, 692−697.

(22) Kloser, E.; Gray, D. G. Surface Grafting of Cellulose Nanocrystals with Poly (ethylene oxide) in Aqueous Media. *Langmuir* **2010**, *26*, 13450−13456.

(23) Cheung, C. C. Y.; Giese, M.; Kelly, J. A.; Hamad, W. Y.; MacLachlan, M. J. Iridescent Chiral Nematic Cellulose Nanocrystal/polymer Composites Assembled in Organic Solvents. *ACS Macro Lett.* **2013**, *2*, 1016−1020.

(24) Beck, S.; Bouchard, J.; Berry, R. Controlling the Reflection Wavelength of Iridescent Solid Films of Nanocrystalline Cellulose. *Biomacromolecules* **2011**, *12*, 167−172.

(25) Beck, S.; Bouchard, J.; Chauve, G.; Berry, R. Controlled Production of Patterns in Iridescent Solid Films of Cellulose Nanocrystals. *Cellulose* **2013**, *20*, 1401−1411.

(26) Kelly, J. A.; Yu, M.; Hamad, W. Y.; MacLachlan, M. J. Large, Crack-free Freestanding Films with Chiral Nematic Structures. *Adv. Opt. Mater.* **2013**, *1*, 295−299.

(27) Dong, X. M.; Kimura, T.; Revol, J. F.; Gray, D. G. Effects of Ionic Strength on the Isotropic−chiral Nematic Phase Transition of Suspensions of Cellulose Crystallites. *Langmuir* **1996**, *12*, 2076−2082.

(28) Liu, D.; Wang, S.; Ma, Z.; Tian, D.; Gu, M.; Lin, F. Structure-color Mechanism of Iridescent Cellulose Nanocrystal Films. *RSC Adv.* **2014**, *4*, 39322−39331.

(29) Khan, M. K.; Giese, M.; Yu, M.; Kelly, J. A.; Hamad, W. Y.; MacLachlan, M. J. Flexible Mesoporous Photonic Resins with Tunable Chiral Nematic Structures. *Angew. Chem., Int. Ed.* **2013**, *52*, 8921−8924.

(30) Parag, K.; Rangaramanujam, M. K. Improvement in Ductility of Chitosan through Blending and Copolymerization with PEG: FTIR Investigation of Molecular Interactions. *Biomacromolecules* **2003**, *4*, 173−180.

(31) Mansur, H. S.; Oréfice, R. L.; Mansur, A. A. P. Characterization of Poly(vinyl alcohol)/poly(ethylene glycol) Hydrogels and PVA-derived Hybrids by Small-angle X-ray Scattering and FTIR Spectroscopy. *Polymer* **2004**, *45*, 7193−7202.

(32) Zhang, Y.; Kohler, N.; Zhang, M. Surface Modification of Superparamagnetic Magnetite Nanoparticles and Their Intracellular Uptake. *Biomaterials* **2002**, *23*, 1553−1561.

(33) Shao, C. L.; Kim, H. Y.; Gong, J.; Lee, D. A Novel Method for Making Silica Nanofibres by Using Electrospun Fibres of Poly-vinylalcohol/silica Composite as Precursor. *Nanotechnology* **2002**, *13*, 635−637.

(34) Xia, J.; Song, L. X.; Dang, Z.; Shao, Z. C. Polyethylene Glycol/Fe3O4 Nanoparticle Composite Materials: Structure, Physical Properties and Application. *Acta Physico-Chimica Sinica* **2013**, *29*, 1524−1533.

(35) Hamley, I. W.; Krysmann, M. J. Effect of PEG Crystallization on the Self-assembly of PEG/peptide Copolymers Containing Amyloid Peptide Fragments. *Langmuir* **2008**, *24*, 8210−8214.

(36) Liu, D.; Li, J.; Sun, F.; Xiao, R.; Guo, Y.; Song, J. Liquid Crystal Microphase Separation of Cellulose Nanocrystals in Wet-spun PVA Composite Fibers. *RSC Adv.* **2014**, *4*, 30784−30789.

(37) Gray, D. G.; Mu, X. Y. Chiral Nematic Structure of Cellulose Nanocrystal Suspensions and Films; Polarized Light and Atomic Force Microscopy. *Materials* **2015**, *8*, 7873−7888.